

Migration behavior of magnetic nanoparticles with chain-like structure under gradient magnetic field and its influence on magnetic hyperthermia

Yundong Tang(汤云东), Xiaoyi Yang(杨晓艺), Rodolfo C.C. Flesch(弗莱施 C.C.鲁道夫), and Tao Jin(金涛)
Citation: Chin. Phys. B, 2026, 35 (**5**): 058701. DOI: 10.1088/1674-1056/ae0899
http://cpb.iphy.ac.cn; http://iopscience.iop.org/cpb

What follows is a list of articles you may be interested in

Effect of different injection strategies considering intravenous injection on combination therapy of magnetic hyperthermia and thermosensitive liposomes

Jiajia Zhu(朱佳佳), Yundong Tang(汤云东), Rodolfo C. C. Flesch(弗莱施 C. C. 鲁道夫), and Tao Jin(金涛)
Chin. Phys. B, 2024, 33 (**12**): 128703. DOI: 10.1088/1674-1056/ad8a48

Detection of HIV-1 antigen based on magnetic tunnel junction sensors

Li Li(李丽), Kai-Yu Mak(麦启宇), Yan Zhou(周艳)
Chin. Phys. B, 2020, 29 (**8**): 088701. DOI: 10.1088/1674-1056/ab928d

Rare earth permanent magnets prepared by hot deformation process

Ren-Jie Chen(陈仁杰), Ze-Xuan Wang(王泽轩), Xu Tang(唐旭), Wen-Zong Yin(尹文宗), Chao-Xiang Jin(靳朝相), Jin-Yun Ju(剧锦云), Don Lee(李东), A-Ru Yan(闫阿儒)
Chin. Phys. B, 2018, 27 (**11**): 117504. DOI: 10.1088/1674-1056/27/11/117504

Effect of particle size distribution on magnetic behavior of nanoparticles with uniaxial anisotropy

S Rizwan Ali, Farah Naz, Humaira Akber, M Naeem, S Imran Ali, S Abdul Basit, M Sarim, Sadaf Qaseem
Chin. Phys. B, 2018, 27 (**9**): 097503. DOI: 10.1088/1674-1056/27/9/097503

Development of MEMS-based micro capacitive tactile probe

Lei Li-Hua (雷李华), Li Yuan (李源), Fan Guo-Fang (范国芳), Wu Jun-Jie (吴俊杰), Jian Li (简黎), Cai Xiao-Yu (蔡潇雨), Li Tong-Bao (李同保)
Chin. Phys. B, 2014, 23 (**11**): 118703. DOI: 10.1088/1674-1056/23/11/118703

Migration behavior of magnetic nanoparticles with chain-like structure under gradient magnetic field and its influence on magnetic hyperthermia

Yundong Tang(汤云东)[1,†], Xiaoyi Yang(杨晓艺)[1], Rodolfo C.C. Flesch(弗莱施 C.C. 鲁道夫)[2], and Tao Jin(金涛)[3]

[1] *College of Physics and Information Engineering, Fuzhou University, Fuzhou* 350108, *China*
[2] *Departamento de Automação e Sistemas, Universidade Federal de Santa Catarina*, 88040-900 *Florianópolis, SC, Brazil*
[3] *College of Electrical Engineering and Automation, Fuzhou University, Fuzhou* 350108, *China*

(Received 4 August 2025; revised manuscript received 16 September 2025; accepted manuscript online 18 September 2025)

Magnetic hyperthermia uses magnetic nanoparticles (MNPs) to generate the heat used for damaging cancer cells under an alternating magnetic field. In fact, the MNPs tend to gather at the injection center and also occur the clustering phenomenon at the same time when injecting into tumor tissue, which however can ultimately result in the excessive concentration of heat in the injection site. Thus, this study aims at improving the MNPs concentration distribution after the injection behavior by considering the action of a static gradient magnetic field, and finally optimizes both temperature situation and thermal damage degree for tumor tissue during magnetic hyperthermia. The MNPs distribution inside a proposed liver tumor is simulated by adopting a Monte Carlo method with adaptive step size, which consists of enough number of small size particles used to analyze the behavior of migration, diffusion, and chain-like phenomenon. The research results demonstrate that the introduction of static gradient magnetic field can disperse the MNPs and form a chain-like distribution inside tumor, and can then expand the distribution range of MNPs, thereby optimizing the thermal damage degree of tumor tissue. In addition, a PID controller with proper setting coefficients is also proven to be able to improve the therapeutic effect for hyperthermia by shortening the rising time to the critical temperature when proper coefficients are set properly during therapy.

Keywords: magnetic hyperthermia, magnetic nanoparticles, particles migration, gradient magnetic field

PACS: 87.85.Qr, 75.50.Tt, 82.70.Dd

DOI: 10.1088/1674-1056/ae0899 **CSTR:** 32038.14.CPB.ae0899

1. Introduction

Magnetic hyperthermia, as an emerging tumor technology, can induce the apoptosis of tumor cells when the temperature exceeds the tolerance threshold of tumor tissues.[1,2] The temperature elevation required for therapy is obtained by the heat production released from magnetic nanoparticles (MNPs) after exposing to an alternating magnetic field.[3] Since the MNPs are transported into tumor area by the injection behavior for ferrofluid before magnetic hyperthermia, so their concentration distributions inside tumor are related to several elements including the injection behavior and the feature of nanofluid and biological tissue.[4,5] Thus, the MNPs concentration distribution inside tumor is significantly relevant to the therapeutic temperature and ultimately lead to the thermal injury of tumor cells during magnetic hyperthermia. Although previous reports have made the relevant research on magnetic hyperthermia, the model for MNPs distribution still lacks enough attention.

In fact, several researches generally defined a given value for the power consumption of MNPs used for therapy, and ignored the existence of particles in their models for the sake of simplicity.[6,7] Wu *et al*. proposed a bi-layered spherical model to simulate the biological tissue with tumor during magnetic hyperthermia, in which the MNPs is constructed as a sphere inside tumor for therapy.[8] However, this method does differ significantly from the actual situation. Tang *et al*. proposed 64 individual MNPs inside tumor to represent the MNPs distribution for a three-dimensional (3D) biological model, in which MNPs are designed to three different shapes in order to validate different treatment effects.[9] In order to present more real situation, researchers simulated the concentration distribution for nanofluid based on an original experimental image according to previous literature.[10] Although these studies have made significant contributions to the establishment of MNP models, there still exists several shortages, such as the number of MNPs and the interaction of different MNPs. In addition, Zhao *et al*. studied the characteristics of magnetization dynamics and energy dissipation for MNPs in static and alternating magnetic fields through Brownian dynamics, and revealed that static magnetic field can improve MNPs dissipation and enhance heat generation efficiency.[11] Furthermore, the static magnetic field induces the dipole interactions between particles, and leads to the formation of chain-like structure along the direction of magnetic field.[12,13] This chain-

†Corresponding author. E-mail: tangyundong@fzu.edu.cn

© 2026 Chinese Physical Society and IOP Publishing Ltd. All rights, including for text and data mining, AI training, and similar technologies, are reserved.

like structure can not only increase the specific absorption rate of MNPs, but also may alter the temperature uniformity of thermal therapy area according to previous literature.[14] In addition to the chain-like characteristics, a static magnetic field with gradient can also result in the migration and diffusion towards high magnetic field regions,[15] and the gradient magnitude can directly affect the migration and aggregation of MNPs due to the force from gradient difference.[16] Previous researchers have found that diffusion mainly occurs in low gradient field, while high gradient field are more conducive to MNPs aggregation.[17,18] However, few of previous reports concerned on the effect of static gradient field on the MNPs distribution inside bio-tissue, and also did not further associate this influencing factor with the thermal damage behavior during magnetic hyperthermia.

In view of the above situation, this study simulates the MNPs distribution by introducing a more efficient adaptive Monte Carlo method for a proposed liver tissue with tumor, in which the MNPs achieve the clustering and diffusion behavior under a static gradient magnetic field. The thermal damage behavior for tumor cells is investigated between different MNPs distributions with and without considering the static magnetic field with gradient. Compared to traditional Monte Carlo method, the proposed adaptive method can cover both converge faster and simulation speed by considers the adaptive step size. In addition, a PID controller with proper setting coefficients is also used to improve the thermal damage degree by increasing the effective treatment time during magnetic hyperthermia.

2. Methodology

2.1. Particle chain-like model

MNPs can form magnetic dipoles under the action of an applied static magnetic field, which can generally generate dipole forces on each other. Besides, MNPs should also affected by many other forces, such as the viscous resistance of magnetorheological fluid, repulsive force, Brownian force, van der Waals force, gravitational potential energy and also buoyancy.[19] In addition, the magnetic moment of MNPs tends to form a chain of particles aligned along the direction of the magnetic field after applying a static magnetic field, which is profit to the reduction of the system energy and ultimately maintains the system to be a more stable state.

In terms of system energies, the main system energies considered in this method consists of the magnetic interaction energy from MNPs, E_{M}, the static magnetic field energy, E_{H}, the resistance energy generated by surfactant molecules, E_{S}, and the van der Waals potential energy, E_{V}.[20] The magnetic interaction energy can be expressed as[21]

$$E_{\mathrm{M}} = \frac{\mu_0 \left[\boldsymbol{m}_i \cdot \boldsymbol{m}_j \cdot D^2 - 3\left(\boldsymbol{m}_i \cdot \boldsymbol{D}\right)\left(\boldsymbol{D} \cdot \boldsymbol{m}_j\right)\right]}{4\pi D^5}, \tag{1}$$

where subscripts i and j denote the particle number, constant, μ_0 denotes the vacuum permeability, which is generally taken as $4\pi \times 10^{-7}$ H/m. Parameters $\boldsymbol{m}$, D, and $\boldsymbol{D}$ indicate the magnetic moment of particle, the center distance of two particles, and the centers distance vector of two particles. The static magnetic field energy have an expression as follows:[22]

$$E_{\mathrm{H}} = -\boldsymbol{m}_i \cdot \boldsymbol{H}, \tag{2}$$

where $\boldsymbol{H}$ denotes the strength of static magnetic field. When the particle surfaces are too close together, the active agent molecules on the particle surfaces will repel each other and then result in the resistance energy with the following expression:[21]

$$E_{\mathrm{S}} = -2\pi d^2 \gamma \left[\left(\frac{D}{\varepsilon} - 2\right) \ln\left(2 - \frac{d}{D - 2\varepsilon}\right) + \frac{D-d}{\varepsilon}\right] kT_0, \quad (0 \le D - d \le 2\varepsilon), \tag{3}$$

where variables d, γ, ε, k, T_0 represent the particle size, the number of active agent molecules adsorbed per unit of particle surface, the thickness of active agent molecules, Boltzmann's constant (1.38×10^{-23}), the local temperature. In addition, the van der Waals potential energy can be expressed as[21]

$$E_{\mathrm{V}} = -\frac{A}{3}\left[\frac{1}{L^2+4L} + \frac{1}{(L+2)^2} + \ln\frac{\sqrt{L^2+4L}}{L+2}\right], \tag{4}$$

where parameter L is denoted as $L = (D - d - 2\varepsilon)/d$, and A is Hamaker's constant taken as 10^{-19}.

The total potential energy, E, is the sum of four energies with the following expression:

$$E = \sum E_{\mathrm{M}} + \sum E_{\mathrm{H}} + \sum E_{\mathrm{S}} + \sum E_{\mathrm{V}}. \tag{5}$$

2.2. MNPs heat generation model

MNPs can release the heat used for therapy due to the energy loss after being exposed an alternating magnetic field. The energy loss of magnetic particles can mainly have two different mechanisms, hysteresis loss and relaxation loss. The former will play a leading role for larger particle sizes with multi-domain structure, and the latter should be in a dominant position for small particle sizes with super-paramagnetism. In this study, the particles size is designed to be nano level, so the heat generation for MNPs can be predicted by relaxation loss, which further consists of Brownian relaxation due to the friction heat between the particle rotating with the magnetic field and the medium, and Néel relaxation due to the magnetic moment change after the magnetic field flip. Thus, the heat production power by two types of relaxation losses can be calculated by Rosensweig's theory with the following expression:[3,23]

$$P_{\mathrm{MNP}} = \frac{\omega^2 \mu_0 \chi_0 \tau_{\mathrm{eff}} H_0^2}{2 + 2\omega^2 \tau_{\mathrm{eff}}^2}, \tag{6}$$

where variables μ_0, H_0, χ_0 represent the vacuum permeability, the strength of alternating magnetic field, the equilibrium magnetization rate, respectively. The angular frequency of magnetic field can be denoted as $\omega = 2\pi f_{\mathrm{AM}}$, where f_{AM} is the frequency of magnetic field. The effective relaxation time, τ_{eff}, caused by Brownian and Néel relaxation can be denoted as[24]

$$\tau_{\mathrm{eff}} = (\tau_{\mathrm{B}} \cdot \tau_{\mathrm{N}})/(\tau_{\mathrm{B}} + \tau_{\mathrm{N}}), \tag{7}$$

where both τ_{B} and τ_{N} have their further expressions as[25] $\tau_{\mathrm{B}} = (\pi\bar{\omega}d_{\mathrm{H}}^3)/(2\kappa T_0)$ and $\tau_{\mathrm{N}} = \tau_0 \exp(\sigma\pi d^3)/(6\kappa T_0)$. Parameters $\bar{\omega}$, d_{H}, σ, τ_0 represent the kinetic viscosity of magnetic fluid, the kinetic diameter of particle, the particle magnetic anisotropy constant, the attempt time.

2.3. Thermal damage model based on therapeutic temperature

During magnetic hyperthermia, magnetic nanoparticles are injected into biological tissues and then generate the heat for therapy after the action of alternating magnetic field. The elevation of therapeutic temperature is determined by several factors, which can usually be predicted by a well-known biological heat transfer equation by Pennes according to previous literature[26,27]

$$\begin{cases} \rho_{\mathrm{T}} c_{\mathrm{T}} \dfrac{\partial T}{\partial t} = k_{\mathrm{T}} \nabla^2 T - Q_{\mathrm{B}} + Q_{\mathrm{m,T}} + \alpha Q_{\mathrm{MNP}}, \\ \rho_{\mathrm{h}} c_{\mathrm{h}} \dfrac{\partial T}{\partial t} = k_{\mathrm{h}} \nabla^2 T - Q_{\mathrm{B}} + Q_{\mathrm{m,h}}, \end{cases} \tag{8}$$

where subscript "T" and "h" refer to the corresponding parameters for tumor and healthy tissue, respectively. Variables ρ, c, k, T, Q_{m}, α are used to represent the density, the specific heat capacity, the thermal conductivity, the temperature, the heat of metabolism, and modification coefficient, respectively. The power release of all MNPs inside tissue, Q_{MNP}, can be converted to the P_{MNP} by the expression as $Q_{\mathrm{MNP}} = \phi P_{\mathrm{MNP}}$, where ϕ indicates the volume fraction. The convective cooling of blood perfusion is specifically denoted by

$$Q_{\mathrm{B}} = \rho_{\mathrm{b}} c_{\mathrm{b}} \omega_{\mathrm{b}} \Delta T, \tag{9}$$

where subscript "b" refers to the feature for blood, and ω_{b} is the blood perfusion rate. Symbol ΔT is the temperature difference between the tissue and the blood.

Equation (8) can be calculated by using finite element method, in which proper original and limit conditions will be helpful to the convergence of results. For example, the initial temperature of biological tissue should be set to the body temperature in healthy case, and the boundary temperature of different tissues should be continuous according to Neumann boundary condition,[10] as follows:

$$\begin{cases} T_{\mathrm{T}}|_{t=0} = T_{\mathrm{h}}|_{t=0} = 37\ ^{\circ}\mathrm{C}, \\ T_{\mathrm{T}}|_{\Psi} = T_{\mathrm{h}}|_{\Psi}, \end{cases} \tag{10}$$

where Ψ denotes the boundary between tumor and liver tissue.

Generally, the temperature of tolerance threshold for tumor cells is 42 °C while is 46 °C for healthy tissue. That also means the temperature scale between 42 °C and 46 °C can effectively damage tumor cells but not the healthy bio-tissue during magnetic hyperthermia. This study considers CEM43 model to quantify the thermal damage for biological tissue, which can be used to convert the heating time at different temperature into the equivalent time at 43 °C with the following expression:[28]

$$\mathrm{CEM43} = \int_0^{t_0} R^{43-T(t)}\,\mathrm{d}t, \tag{11}$$

where $T(t)$ refers to the temperature at a specific time t. The compensation coefficient R is used to indicate the degree of tissue thermal damage due to different heating temperatures, which be expressed as

$$\begin{cases} R = 0.25, & T < 43\ ^{\circ}\mathrm{C}, \\ R = 0.5, & T > 43\ ^{\circ}\mathrm{C}. \end{cases} \tag{12}$$

2.4. Adaptive Monte Carlo method

This study introduces an adaptive Monte Carlo method to simulate chain-like distribution for MNPs under the action of an external gradient magnetic field. Monte Carlo method is a common mathematical simulation method, which realizes random sampling and statistical simulation by randomly repeating experiments and approximates the real results by probabilistic statistics.[22] This study mainly adopts the acceptance-rejection sampling method, which is one of three main sampling methods in Monte Carlo method.

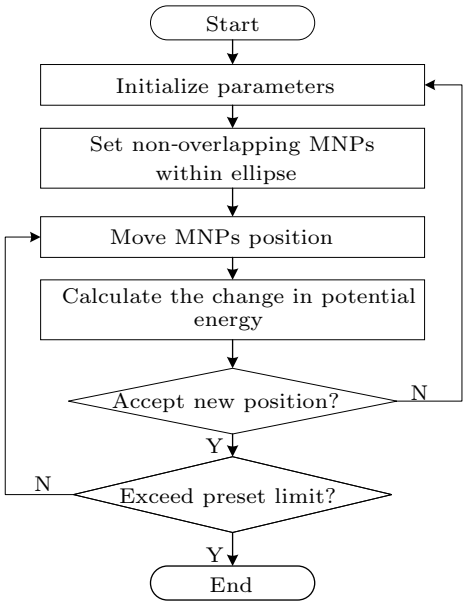


Fig. 1. MNPs modeling procedure using Monte Carlo simulation.

Figure 1 presents the flowchart of Monte Carlo simulation method for MNPs chain-like distribution under the gradient magnetic field. Initialize all parameters, which consist of

ellipse tumor size ($a \times b$), particle size (d), particles number (num), and the upper limit of cycle (N); Set the position of ellipse, and makes the initial MNPs have a normal distribution at the ellipse center while do not overlap with each other and exceed the elliptical boundary; Move the position of particle i and save the particles coordinates (x_i, y_i) before and after moving; Calculate the difference of potential energy before and after moving as, $\Delta E = E_{\text{old}} - E_{\text{new}}$; Produce a random number Z, homogeneously distributed in [0,1], and then obtain the transfer probability according to Metropolis criterion[29]

$$P = \exp(\Delta E / kT_0), \tag{13}$$

where T_0 is the absolute temperature in unit K. Thus, if $P > Z$, the result of displacement is retained; otherwise, the result is withdrawn, and the cycle number q. In addition, if the number q, has not reached the preset cycle upper limit N, the particle will be moved to a new position $i+1$; Otherwise, jump out of the cycle and complete the particle distribution simulation.

In fact, the key for Monte Carlo simulation is the step-size setting of particle movement.[30] This study adopts an adaptive Monte Carlo method that can dynamically adjust the moving step-size in order to keep the simulated sampling acceptance rate to a range between 0.35 and 0.4 under anisotropic target distribution.[31] The sampling acceptance rate R_e is expressed as $R_e = m/q$, where m and q represent the number of accepted particle displacements and the current total number of cycles. The specific steps for adaptive step-size are as follows: assume that the sampling rate range is set to 30% 50%; the initial step-size is defined to 0.15 d and 0.2 d in the x and y directions due to the more energy changes along the displacement of magnetic field direction;[32] the step-size is reduced to 0.75 times of original step-size in the case with the acceptance rate less than 30%, or is increased to 1.25 times in the case greater than 50%. The acceptance rate is defined as quotient of the number of accepting displacement and the total number of samples, which will be calculated once every 100 samples.

3. Results and discussion

In aim to investigate the influence of the MNPs chain-like structure, this study develops a mouse liver model contained MNPs distribution for magnetic hyperthermia, in which the MNPs model is scaled up 2000 times in order to have a better observation and analysis on results. Meanwhile, the computer burden during simulation can also be decreased greatly. As illustrated in Fig. 3, the proposed model consists of an outline of mouse liver with about 30 mm×20 mm in size based on previous experimental image,[33] an ellipse shape tumor with 10 mm×6 mm, and the MNPs with a particle size of 0.16 mm inside tumor.

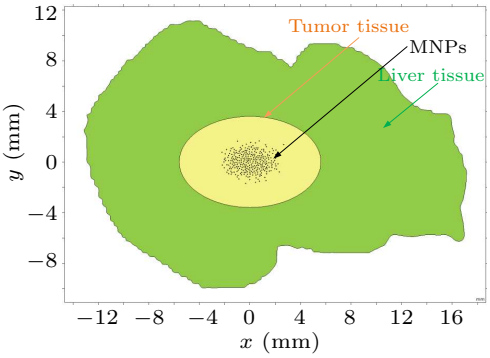


Fig. 2. Proposed liver model including tumor and MNPs.

The key parameters for simulating MNPs distribution using the Monte Carlo method are set as follows: $T_0 = 310$ K, static magnetic field $H_s = 20$ kA/m, the number of active agent molecules adsorbed on particle surface, $\gamma = 400$, the thickness of active agent molecules, $\varepsilon = 1$ nm, the long and short axes of tumor, $a = 5$ mm and $b = 3$ mm. In addition, the parameters required for the bioheat transfer model are also summarized according to previous reports, as illustrated in Table 1.[34]

Table 1. Parameters of hyperthermia materials.

	ρ (kg·m^{-3})	c (J·kg^{-1}·K^{-1})	K_h (W·m^{-1}·K^{-1})	Q_m (W·m^{-3})
Liver	1079	3540	0.52	14414
Tumor	1050	3750	0.59	684.2
Blood	1050	3750	0.59	–
MNPS	5180	670	40	–

3.1. Algorithm analysis

This study considers Monte Carlo method with adaptive step size to simulate MNPs distribution. The sampling acceptance rate of proposed method will be analyzed during the sampling process in order to have a performance comparison to the Monte Carlo method with traditional fixed step. Figure 3 compares the performance of different Monte Carlo methods by the sampling acceptance rate during the sampling process, which are traditional one and an improved adaptive-step-size one, respectively. As can be observed from Fig. 3, the sampling acceptance rate in the adaptive step-size case drops rapidly to about 20% at about 10^4 cycles, and then stabilizes at 3×10^4 cycles after increasing gradually to about 35%. In contrast, the fixed-step case presents a relatively slow downward trend in the initial stage with respect to the adaptive step-size case, which attributes to its relatively slow growth in the step-size but not the exponentially increasing in adaptive step-size case. For the fixed-step Monte Carlo method, the step-size of sampling process always remains constant, and leads to a slow decrease in the sampling acceptance rate. The results demonstrate that compared to the fixed-step-size case, the Monte Carlo method with adaptive step-size can have faster convergence speed, smaller computational load, and faster calculation rate.

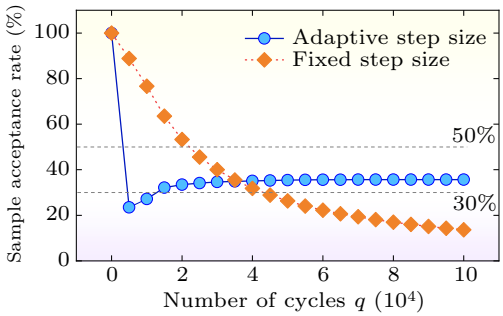


Fig. 3. Sample acceptance rate in Monte Carlo simulation process.

3.2. Magnetic nanoparticles distribution

There are primarily two methods for MNPs to enter the tumor region, intravenous injection and direct injection. The former usually has the disadvantage in low targeting efficiency and systemic particle retention, which can be improved by considering the MNPs with markers.[35] Thus, the direct injection becomes a common practice in most scenarios including this study. MNPs can be injected into the tumor region through a needle, which however generally aggregate near the injection site since they are not easily diffused due to the porous media properties of tumor.[36] This situation can then lead to the overheat phenomenon in the MNPs concentration area and the low power in the MNPs deficiency region during magnetic hyperthermia. For this reason, this study simulates a static gradient magnetic field in the x-axis direction with purposed of optimizing the MNPs distribution for magnetic hyperthermia. This gradient magnetic field is constructed using four matrix coils based on previous literature,[37] as is presented in Fig. 4. It can be understood that the magnetic field intensity gradually grows along the x-axis center towards both ends in Fig. 4(a), which can be observed more clearly in the curve of Fig. 4(b) for the magnetic field value of centerline case. As can be shown in Fig. 4(b), the magnetic field value approximately increases rapidly from the tumor center outward.

Figure 5(a) shows the normal distribution for MNPs inside tumor in the initial state, in which most of the MNPs gather around the injection site of tumor region after the nanofluid injection behavior. Although this normal distribution is more real than a uniform case, it still cannot express the chain-like reaction caused by the cluster behavior. Figure 5(b) illustrate the MNPs distribution after the migration motion due to the static gradient magnetic field, in which the Monte Carlo method is considered for this simulation. As can be seen, the MNPs will be arranged in a chain-like pattern along the direction of magnetic field and migrate towards high magnetic field region under the influence of gradient magnetic fields. In Monte Carlo simulation, the MNPs move randomly at each sampling, and the moved MNPs have lower energy and more stable than that of the dispersed particles when they aggregate in chains along the direction of magnetic field. Thus, the MNPs tend to form a chain-like structure under low magnetic field area, and prefer to migrate to the high region at the same time.

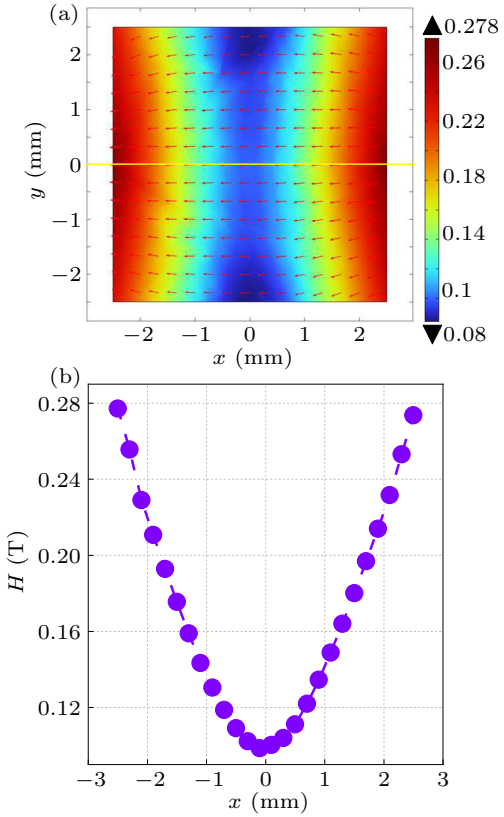


Fig. 4. Gradient magnetic field distribution due to four matrix coils: (a) in xy plane and (b) along centerline.

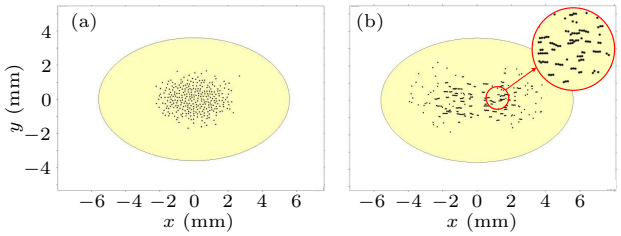


Fig. 5. MNPs distribution inside tumor before and after the static gradient magnetic field: (a) before and (b) after.

3.3. Therapeutic temperature analysis

The static magnetic field can actually affect the heat generation efficiency of MNPs, so it will be removed from the therapeutic target when the magnetic field starts to work.[38] Different MNPs distribution inside tumor can result in different temperature distribution and further different thermal damage for tumor tissue under the same conditions. In order to validate the advantage of the influence of gradient magnetic fields, this study predicts the temperature distribution for tumor area with a heating time of 30 min, in which the power consumption of each MNPs is defined to be a critical value, 2.88×10^6 W/m^3, by an exhaustive method for proposed geometric model. This power for MNPs can guarantee the maximum therapeutic temperature of the proposed model under a critical value, 46 °C, in order to damage the tumor cells but

not the healthy tissue. Figure 6 shows the temperature distribution of biological tissue under the critical power, in which the MNPs after the injection is the initial state of normal distribution. The area inside the 42 °C isoline of temperature can be considered as the effective treatment since this value is the critical value for the damage of tumor cells during magnetic hyperthermia. Although figure 6(a) presents the overall view of therapeutic temperature distribution for the proposed model, the local enlarged image of tumor area in Fig. 6(b) can illustrate the results more clearly. Thus, this study will present all the results using the local enlarged image in the following text. As can be illustrated from Fig. 6(b), the shape of temperature distribution is almost agreed with the MNPs distribution, in which both MNPs and heat are concentrated in the central area and decrease away from the center of tumor area. In addition, it can be easily obtained that the area with temperature greater than 42 °C accounts for 22.53% of total tumor area at this time.

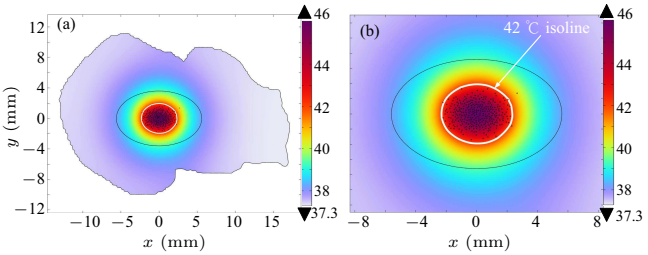


Fig. 6. Therapeutic temperature distribution for biological tissue considering the MNPs with normal distribution under different views: (a) whole view and (b) local enlarged view.

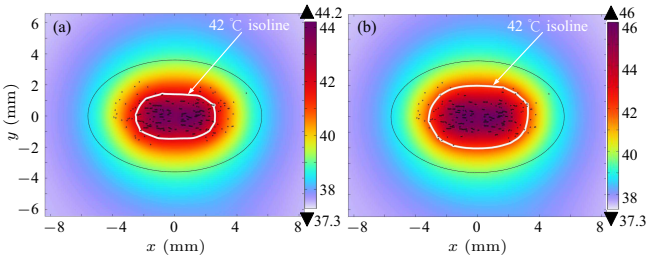


Fig. 7. Temperature distribution for the case considering the static gradient magnetic field under different heat generations for MNPs: (a) 2.88×10^6 W/m^3 and (b) 3.68×10^6 W/m^3.

When the same condition is applied to the case considering the application of static gradient magnetic field, the temperature distribution for therapy will change with the migration of MNPs inside tumor, as is described in Fig. 7(a). As can be understood from Fig. 7(a), the highest temperature drops to a lower value, 44.2 °C, and the percentage of tumor area above 42 °C drops to 19.61% with the 42 °C isoline changing from the approximately circular shape to an almost elliptical shape. In order to improve the therapeutic effect for this case, this study appropriately increases the heat generation power for MNPs while does not damage the healthy tissue. As is illustrated in Fig. 7(b), the maximum tissue temperature for the case considering the static gradient magnetic field is increased to the critical value, 46 °C, again after improving the power dissipation for MNPs to 3.68×10^6 W/m^3. It is worth mentioning that the effective percentage of treated area to tumor area significantly improved to 33.69%, which is increased by about 50% with respect to the case presented in Fig. 6.

3.4. Thermal damage analysis

Continuous heating with specific therapeutic temperature can effectively damage the tumor cells, and the degree of this irreversible damage can generally be evaluated by CEM43 value during magnetic hyperthermia. Figure 8 shows the CEM43 value situation considering the initial normal distribution, which is basically consistent with the trend of therapeutic temperature distribution illustrated in Fig. 6. As can be observed, the maximum value of CEM43 in this case in 239 min, which is far greater than the critical value for the liver damage, 9.9 min, based on previous report.[36] In addition, the irreversible thermal damage area greater than 9.9 accounts for 20.44% of total tumor area at this time.

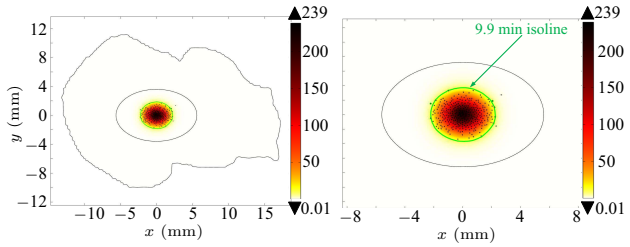


Fig. 8. CEM43 profile for biological tissue considering the MNPs with normal distribution under different views: (a) whole view and (b) local enlarged view.

Similarly, figure 9 describes the CEM43 value situation for the MNPs distribution considering the static gradient magnetic field, in which the maximum value decreases from 239 min for the initial case to 74.5 min and the effective area percentage of irreversible thermal damage drop sharply to 17.09%. Therefore, the migration and cluster behavior due to the static gradient magnetic field disperses the heat for biological tissue and decreases the irreversible damage to the tumor tissue at the same time when the same input power of MNPs is considered for therapy during magnetic hyperthermia. Similar to the therapeutic temperature, this adverse situation for thermal damage can also be effectively improved when the heat power for MNPs is defined to a new threshold value. As can be observed from Fig. 9(b), the maximum CEM43 increases from 74.5 min to 368 min, and the effective area percentage of irreversible thermal damage effectively increases to a greater value, 30.54%, at this time. This area percentage is about 1.5 times more than the case without considering the static gradient magnetic field. Thus, it can be concluded that the migration behavior due to the static gradient field can lead to the heat dispersion and further the damage reduction, which can in fact be optimized by increasing the proper heat production for MNPs.

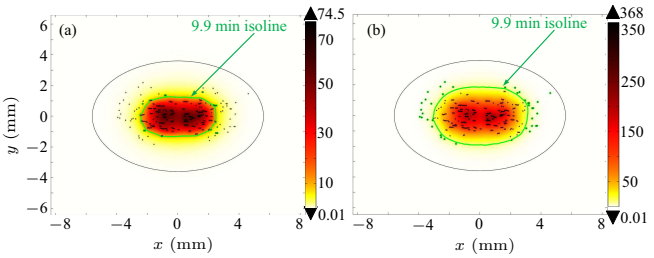


Fig. 9. CEM43 profile for the case considering the static gradient magnetic field under different heat generations for MNPs: (a) 2.88×10^6 W/m^3 and (b) 3.68×10^6 W/m^3.

3.5. Proposed optimization method for therapeutic temperature

As described above, the therapeutic effect can be improved effectively by the proposed optimization method considering the static gradient field and the critical power at the same time. Nevertheless, the treatment time can in fact be optimized further to improve the thermal damage for tumor cells since too excessive time is harmful to human body. The ideal situation for hyperthermia is to have as much time and temperature as possible, while this point has not been concerned in previous discussion. Thus, this study considers a PID controller for the magnetic hyperthermia system, which can quickly increase the temperature of malignant area to the specified critical value 46 °C, in order to simultaneously increase both the effective time and the temperature. The PID algorithm is a classic control strategy including proportional, integral, and derivative, which achieves the precise control by feeding back data errors to the control system. The output of PID controller is represented as

$$u(t) = K_{\mathrm{p}}\left(T_{\mathrm{set}}-T\left(t\right)\right)+K_{\mathrm{i}}\int_0^t\left(T_{\mathrm{set}}-T\left(\tau\right)\right)\mathrm{d}\tau + K_{\mathrm{d}}\frac{\mathrm{d}\left(T_{\mathrm{set}}-T\left(t\right)\right)}{\mathrm{d}t}, \tag{14}$$

where parameters K_{p}, K_{i}, K_{d}, T_{set}, $T(t)$ represent proportional, integral, and differential coefficients, the critical temperature, and the current temperature value, respectively. In addition, the $u(t)$ is used to regulate the treatment temperature of tumor center by the power dissipation of MNPs, Q_{MNP}, in Eq. (8). In order to obtain a set of proper parameters, the trial-and-error method is considered for this study during the debugging process. These three coefficients with an initial state of zero are regulated to a proper value sequentially according to improve the response speed, the steady-state error, and the stability of system, which corresponding to different coefficients, K_{p}, K_{i}, K_{d}, respectively. Thus, the temperature of center tumor with maximum value can be controller below a safety value by this proposed PID method. Figure 10 illustrates the temperature change of tumor center over time with and without the PID algorithm, in which three sets of coefficients are taken into consideration for adjusting. As can be observed, when both K_{p} and K_{d} are determined, parameter K_{i} can affect the degree of oscillate and overshoot. In this situation, the time required for the temperature to reach a stable state is shortened from 225 s before PID to about 40 s. in addition, the overshoot is 6.63% in $K_{\mathrm{i}}=1$, is 3.69% in $K_{\mathrm{i}}=0.5$, and a more ideal 0.2% in the case of $K_{\mathrm{i}}=0.1$. Thus, when the PID algorithm with proper coefficients is considered, the thermal damage of tumor tissue can be improved by effectively raising the effective treatment time for therapy.

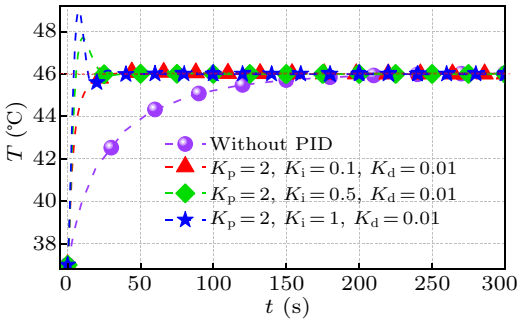


Fig. 10. Tumor center temperature over time under different PID coefficients.

4. Conclusion

This study simulates the MNPs distribution under the static gradient magnetic field, and investigates the effect of MNPs migration behavior on both therapeutic temperature situation and thermal damage degree during magnetic fluid hyperthermia. The analysis results show that MNPs can migrate towards the high magnetic field region and form chain-like structure along the direction of magnetic field when are exposed to the gradient magnetic field before magnetic hyperthermia, which has also been confirmed in the experimental results presented in previous references.[15,16] Furthermore, this migration and diffusion behavior can then result in a decrease in the overall temperature and an increase in the range of temperature elevation during therapy, which however reduce the overall therapeutic temperature value due to the MNPs diffusion with the gradient magnetic field at the same time. In this process, the area percentage of therapeutic temperature greater than 42 °C decreases from 22.53% in the initial case to 19.61% in the case considering the gradient field, and the effective percentage for thermal damage reduces from 20.44% in the initial case to 17.09% in the case after the diffusion behavior accordingly. The emergence of this situation can also be foreseen from the core content described in Ref. [17]. In addition, the results also demonstrate that the proper elevation in the power dissipation for MNPs can effectively improve the treatment effect by both treatment temperature and thermal damage for tumor region during therapy. Meanwhile, the PID controller can also be used to decrease the rising time to 46 °C from 225 s to 40 s under 0.2% of the overshoot rate for the maximum temperature, thereby achieving a significant improvement for the thermotherapy effect. This study investigates the distribution

structure of MNPs under the gradient magnetic field from a microscopic perspective and further analyzes the influence of MNPs distribution on magnetic hyperthermia, which provides a new idea for magnetic hyperthermia in the improvement of treatment effectiveness. Unfortunately, this article was unable to conduct the physical experiments for verification due to limited condition, and the same experimental method as this study has also not been reported in previous clinical trial of magnetic hyperthermia. The subsequent experimental verification for this study is expected to further confirm the correctness and effectiveness of this method.

Acknowledgements

Project supported in part by the National Natural Science Foundation of China (Grant Nos. 62471144 and 62071124) and in part by the Conselho Nacional de Desenvolvimento Científico e Tecnológico (BR) (CNPq) (Grant No. 315546/2021-2).

References

[1] Zhang Y F and Lu M 2024 *Front. Bioeng. Biotechnol.* **12** 1432189
[2] Andreozzi A, Brunese L, Cafarchio A, Netti P and Vanoli G P 2025 *Int. J. Therm. Sci.* **208** 109428
[3] Tang Y D, Chen M, Flesch R C C and Jin T 2023 *Chin. Phys. B* **32** 094401
[4] Ferrero R, Vicentini M and Manzin A 2024 *Nanoscale Adv.* **6** 1739
[5] Jiang Q, Ren F, Wang C L, Wang Z K, Kefayati G, Kenjeres S, Vafai K, Cui X G, Liu Y and Tang H 2025 *Int. J. Heat Mass Transfer* **245** 126982
[6] Kandala S K, Liapi E, Whitcomb L L, Attaluri A and Ivkov R 2019 *Int. J. Hyperthermia* **36** 115
[7] Valente A, Loureiro F, Di Bartolo L and Mansur W J 2018 *Int. Commun. Heat Mass Transfer* **91** 248
[8] Wu L, Cheng J J, Liu W Z and Chen X G 2015 *IEEE Trans. Magn.* **51** 1
[9] Tang Y D, Flesch R C C, Jin T, Gao Y M and He M H 2021 *J. Phys. D: Appl. Phys.* **54** 165401
[10] Tang Y D, Wang Y S, Flesch R C C and Jin T 2023 *J. Phys. D: Appl. Phys.* **56** 145402
[11] Zhao Z Y and Rinaldi C 2018 *J. Phys. Chem. C* **122** 21018
[12] Myrovali E, Papadopoulos K, Iglesias I, Spasova M, Farle M, Wiedwald U and Angelakeris M 2021 *ACS Appl. Mater. Interfaces* **13** 21602
[13] Park M, Le T A, Hadadian Y and Yoon J 2022 *J. Magn. Magn. Mater.* **564** 170110
[14] Sanz B, Cabreira-Gomes R, Torres T E, Valdés D P, Lima E, Jr., De Biasi E, Zysler R D, Ibarra M R and Goya G F 2020 *ACS Appl. Nano Mater.* **3** 8719
[15] Manshadi M K D, Saadat M, Mohammadi M, Kamali R, Shamsi M, Naseh M and Sanati-Nezhad A 2019 *Drug Deliv.* **26** 120
[16] Ku J G, Xia J, Li J Z, Peng X L, Guo B and Ran H X 2021 *Powder Technol.* **394** 767
[17] Sharyna S G and Krakov M S 2024 *J. Magn. Magn. Mater.* **599** 172095
[18] Hafez A, Liu Q and Santamarina J C 2023 *Geoen. Sci. Eng.* **228** 212029
[19] Li W M, Ouyang J and Zhuang X 2016 *Soft Mater.* **14** 87
[20] Guo S L, Yi W T and Li Z Z 2023 *Chin. Phys. B* **32** 050203
[21] Montazeri R 2013 *Int. J. Eng.* **26** 99
[22] Liu Y Z, Liu X H and Liu H 2011 *Procedia Eng.* **15** 3896
[23] Rosensweig R E 2002 *J. Magn. Magn. Mater.* **252** 370
[24] Tang Q Q, Lei H, Wu R Q, Fan H M and Lü Y 2021 *Chin. Sci. Bull.* **66** 3462
[25] Yu X, Mi Y, Wang L C, Li Z R, Wu D A, Liu R S and He S L 2021 *Chin. Phys. B* **30** 017503
[26] Tang Y D, Jin T and Flesch R C C 2017 *IEEE Trans. Magn.* **53** 1
[27] Zhu J J, Tang Y D, Flesch R C C and Jin T 2024 *Chin. Phys. B* **33** 128703
[28] Tang Y D, Wang Y S, Flesch R C C and Jin T 2023 *J. Therm. Biol.* **118** 103747
[29] Metropolis N and Ulam S 1949 *J. Am. Stat. Assoc.* **44** 335
[30] Andrieu C and Thoms J 2008 *Stat. Comput.* **18** 343
[31] Haario H, Saksman E and Tamminen J 2001 *Bernoulli.* **7** 223
[32] Bédard M 2008 *Stoch. Process. Appl.* **118** 2198
[33] Pandit H, Tinney J P, Li Y, Cui G Z, Li S P, Keller B B and Martin R C G 2019 *Ultrasound Med. Biol.* **45** 549
[34] Tang Y D, Su H, Flesch R C C and Jin T 2022 *J. Magn. Magn. Mater.* **545** 168730
[35] Farjadian F, Faghih Z, Fakhimi M, Iranpour P, Mohammadi-Samani S and Doroudian M 2023 *Pharmaceutics* **15** 2491
[36] Tang Y D, Zou J, Flesch R C C and Jin T 2023 *Chin. Phys. B* **32** 034304
[37] Yan X H, Li Z X, Sun D, Chen W H and Gao P 2022 *Trans. China Electrotech. Soc.* **37** 4269 (in Chinese)
[38] Sebastian A R, Kim H J and Kim S H 2019 *J. Appl. Phys.* **126** 134902